J. Fluid Mech. (1992), *vol.* 237, *pp.* 373-393
Printed in Great Britain

Optimum plane diffusers in laminar flow

By HAYRI ÇABUK AND VIJAY MODI
Department of Mechanical Engineering, Columbia University, New York, NY 10027, USA

(Received 2 August 1990 and in revised form 27 July 1991)

The problem of determining the profile of a plane diffuser (of given upstream width and length) that provides the maximum static pressure rise is solved. Two-dimensional, incompressible, laminar flow governed by the steady-state Navier–Stokes equations is assumed through the diffuser. Recent advances in computational resources and algorithms have made it possible to solve the 'direct' problem of determining such a flow through a body of known geometry. In this paper, a set of 'adjoint' equations is obtained, the solution to which permits the calculation of the direction and relative magnitude of change in the diffuser profile that leads to a higher pressure rise. The direct as well as the adjoint set of partial differential equations are obtained for Dirichlet-type inflow and outflow conditions. Repeatedly modifying the diffuser geometry with each solution to these two sets of equations with the above boundary conditions would in principle lead to a diffuser with the maximum static pressure rise, also called the optimum diffuser. The optimality condition, that the shear stress all along the wall must vanish for the optimum diffuser, is also recovered from the analysis. It is postulated that the adjoint set of equations continues to hold even if the computationally inconvenient Dirichlet-type outflow boundary condition is replaced by Neumann-type conditions. It is shown that numerical solutions obtained in this fashion do satisfy the optimality condition.

1. Introduction

A shape optimization problem is one in which an objective function defined on a domain and/or on its boundary through the solution of a boundary-value problem, is minimized (or maximized) with respect to the variation of the domain. One problem of this nature is to determine the shape of a body (of given volume) which has minimum drag when moved at constant speed in a viscous fluid. This problem has been addressed, among others by Tuck (1968), Watson (1971) and Pironneau (1973, 1974). The earlier formulations of the problem by Tuck (1968) and Watson (1971) were for a body in Stokes flow. The former led to a numerically intractable integral equation and the later to an estimate of the upper bound on the minimum possible drag. Pironneau (1973), aided by earlier works of Lions (1968) and Lions & Magenes (1967) addressed the same minimum drag problem in Stokes flow for a three-dimensional unit-volume body. It was shown that at optimality the normal derivative of the velocity is constant along the boundary of the body. In addition it was also shown that the general shape of the body is similar to a prolate spheroid with a conical front end and rear ends of angle 120°. However, owing to the lack of a numerical Stokes flow solver, a complete body profile could not be obtained.

In a subsequent study, Pironneau (1974) derived the change in energy dissipation due to a small hump on a body in uniform, steady, laminar flow. Using the above result in conjunction with variational methods of optimal control, 'necessary

optimality conditions' for four minimum-drag problems were obtained. These conditions lead to a set of equations for an additional set of variables called the 'co-state' or the 'adjoint' variables as opposed to the 'direct' variables which are the unknown velocities. The direct variables appear as parameters in the adjoint equations, and hence the direct as well as the adjoint equations together form a coupled set of equations. Because of the complexity of the equations a possible way to solve them is by an iterative numerical procedure. At the time Pironneau (1974) was unable to carry out such a numerical integration. Instead, however, using a boundary-layer assumption he was able to prove that a two-dimensional unit-area body with the smallest drag has a wedge-shaped front end. In a subsequent work Glowinski & Pironneau (1975) presented numerical computations of the minimum-drag profile of a two-dimensional body in laminar flow, although with a Reynolds number large enough (between 1000 and 100000) to permit a boundary-layer approximation. They found that the optimum profile is long and thin with the front end being shaped like a wedge of angle 90° and the rear end like a cusp. While they were unable to compute the detailed body profile, this study to the best of our knowledge comes closest to finding a numerical solution to an optimum design problem in a flow governed by the laminar Navier–Stokes equations. The present study belongs to this class in its theoretical approach with particular emphasis on computation of optimum profiles in the absence of simplifying assumptions such as Stokes flow or thin boundary layers.

Another related class of optimum design problems is the question of determining the profile of a two-dimensional body that will attain a desired surface pressure distribution. The body is assumed to be in otherwise uniform flow. The designer usually has a better understanding of how the performance is related to the pressure distribution than the relationship between the profile and the performance. In a recent survey paper, Jameson (1988) suggests that the design problem be treated as a control problem in which the control is the profile of the boundary. He also provides a comprehensive summary of the earlier related studies in this direction.

In his pioneering contribution Lighthill (1945) solved the problem for incompressible potential flow past a body by conformally mapping it to a unit circle. Similar approaches were used by McFadden (1979) and Garabedian & McFadden (1982) for two- and three-dimensional compressible flow. An alternative formulation of the potential flow design problem is to convert the specified pressure distribution into a corresponding surface speed that can be integrated to obtain the surface potential. Using this potential as the Dirichlet boundary condition to the potential flow equations the profile change can be determined from the computed normal velocity component at the surface. This approach was first suggested by Tranen (1974) and was subsequently used for three-dimensional flow by Henne (1980). Recently, Volpe & Melnik (1986) have demonstrated how to accommodate constraints on the permitted pressure distribution. The problem of design of shock-free transonic airfoils was addressed by Garabedian & Korn (1971) by using the method of complex characteristics to solve the equations in the hodograph plane.

In a significant step towards addressing real flows Giles, Drela & Thompkins (1985) addressed the problem of shape design for flows governed by the two-dimensional Euler equations. They write the two-dimensional Euler equations in a streamline coordinate system and for fixed pressure distribution obtain a Newton solution for the unknown surface coordinates.

Hicks & Henne (1979) have explored the possibility of meeting desired design objectives by using constrained optimization. The configuration is specified by a set

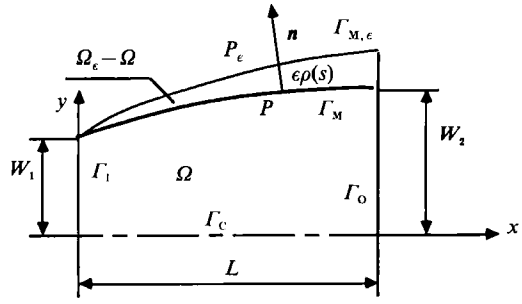

FIGURE 1. Schematic diagram of a plane diffuser. Flow enters at upstream boundary Γ_I and exits at the downstream boundary Γ_O. The wall to be shaped is Γ_M and the symmetry line is Γ_C.

of parameters, flow is solved numerically by a suitable method. The optimization method then selects values of these parameters that maximize some criterion of merit. According to Jameson (1988) this method becomes extremely expensive as the number of parameters is increased, and its successful application in practice depends heavily on the choice of a parametric representation of the configuration.

In the present study optimum design of an internal flow component such as a diffuser in laminar flow is considered. The problem of determining the profile of a plane diffuser (of say, given upstream width and length) that provides the maximum static pressure rise is formulated using a variational method derived from optimal control theory. With careful consideration of the numerical stability of the adjoint equations we have been able to demonstrate the feasibility of optimum design in the context of laminar Navier–Stokes equations without the additional boundary-layer assumption.

2. Statement of the problem

Consider a plane diffuser, as shown in figure 1, of given upstream width W_1 and given length L with incompressible, laminar flow through it. The flow is governed by the incompressible, steady forms of the Navier–Stokes and continuity equations. These are

$$\left.\begin{aligned} u_{i,i} &= 0, \\ u_j u_{i,j} &= -p^*_{,i} + \nu u_{i,jj}, \end{aligned}\right\} \tag{1}$$

where $p^* = p/\rho$. Here u_i, p, ρ, and ν are the velocity components, pressure, density and kinematic viscosity respectively.

A no-slip condition is imposed on the bounding wall. Dirichlet-type boundary conditions are assumed at the entrance and exit; specifically, it is assumed that the streamwise velocity component at the entrance and exit is specified and the transverse velocity component at the entrance and exit is assumed to be zero. Symmetry conditions are assumed at the centreline. Boundary conditions at the entrance and exit then are

$$\left.\begin{aligned} u_1 &= f(y) \quad \text{on} \quad \Gamma_I, \\ u_1 &= g(y) \quad \text{on} \quad \Gamma_O, \\ u_2 &= 0 \quad\;\; \text{on} \quad \Gamma_I \text{ and } \Gamma_O, \end{aligned}\right\} \tag{2}$$

where $f(y)$ and $g(y)$ are assumed to be specified functions. All velocities and lengths are scaled using the average entrance velocity V and the diffuser entrance width

W_1 throughout the paper. Hence the Reynolds number for the flow through the diffuser is defined as $Re = (VW_1)/\nu$.

An appropriate quantity to be minimized or maximized, called the objective function is chosen to formulate the variational problem. One parameter that characterizes the diffuser performance is the static pressure rise through the diffuser. The optimum diffuser profile should be such as to maximize the value of this parameter for a given upstream width and length. Since pressure may vary across the diffuser inlet and exit regions it was decided to choose the change in the flow-weighted integral (over the exit and inlet cross-sectional areas) of the static pressure rise as the objective function. This quantity is given by

$$J(\Gamma_M) = \int_{\Gamma_I} p^* u_i n_i \, ds + \int_{\Gamma_O} p^* u_i n_i \, ds, \tag{3}$$

where n_i is the ith component of the unit normal vector and Γ_M is the portion of the diffuser wall that is to be shaped. The goal then is to determine the diffuser profile that maximizes the above function. The normalized diffuser length, L/W_1 (henceforth simply called the length) is kept constant. The normalized exit width W_2/W_1 (henceforth simply called the exit width) is left arbitrary, and its actual value for the optimum diffuser is part of the solution to the problem and is determined along with the rest of the profile. Since the only mechanism for total pressure drop in the diffuser is viscous dissipation, the optimum profile is also the profile for which the viscous dissipation is a minimum.

3. Mathematical formulation

In this section, the variation of the objective function with respect to the variation of the boundary is obtained by means of a perturbation type of analysis. This analysis follows from arguments not unlike those used for optimum design in potential flow, in an earlier paper by Çabuk & Modi (1990).

First the variation of the solution of the direct problem due to boundary variation is obtained. Let $\rho(s)$ be an arbitrary function of arclength s, defined on Γ_M, and let ϵ be a positive number. Here Γ_M is the part of the boundary that is to be shaped. The whole boundary, including the wall of the diffuser, the centreline and the inlet and exit areas, is denoted by Γ and the domain enclosed by Γ is denoted by Ω. Let each point on Γ_M be moved by $\epsilon\rho(s)$ along the outer normal direction. The curve constructed in this way is denoted by $\Gamma_{M,\epsilon}$ and the new domain is denoted by Ω_ϵ as shown in figure 1. Let $(u_i^\epsilon, p^\epsilon)$ be the solution of (1) in the new domain Ω_ϵ. Let (ϕ_i, π) be defined as follows:

$$\left.\begin{aligned} \phi_i &= \lim_{\epsilon \to 0} \epsilon^{-1} [u_i^\epsilon - u_i] \quad \in \Omega, \\ \pi &= \lim_{\epsilon \to 0} \epsilon^{-1} [p^\epsilon - p^*] \quad \in \Omega. \end{aligned}\right\} \tag{4}$$

Then $(u_i^\epsilon, p^\epsilon)$ can be written as

$$u_i^\epsilon = u_i + \epsilon\phi_i, \quad p^\epsilon = p^* + \epsilon\pi \tag{5}$$

Since both $(u_i^\epsilon, p^\epsilon)$ and (u_i, p^*) satisfy the Navier–Stokes equations, it can be shown that (ϕ_i, π) satisfy the following set of equations:

$$\left.\begin{aligned} \phi_{i,i} &= 0 \\ u_j \phi_{i,j} + \phi_j u_{i,j} &= -\pi_{,i} + \nu \phi_{i,jj} \end{aligned}\right\} \tag{6}$$

In a similar way it can be shown that on the fixed portions of the boundary

$$\phi_i = 0 \quad \text{on} \quad (\Gamma - \Gamma_{\mathrm{M}}) \tag{7}$$

since both u_i^ϵ and u_i satisfy the same boundary conditions.

The next step is to derive the conditions satisfied by ϕ_i on Γ_{M}. Consider a point P on Γ_{M}, and a corresponding point P_ϵ on $\Gamma_{\mathrm{M},\epsilon}$ such that P_ϵ lies on the outward normal $\boldsymbol{n}$, as shown in figure 1. Assume that $\epsilon\rho(s)$ is positive. A Taylor series expansion of u_i^ϵ about the point P, evaluated at $\bar{x} = \bar{x}|_{P_\epsilon}$, along the normal direction $\boldsymbol{n}$ is

$$\begin{aligned} u_i^\epsilon]_{P_\epsilon} &= u_i^\epsilon]_P + \epsilon\rho\left(\frac{\partial u_i^\epsilon}{\partial n}\right)_P + O(\epsilon^2) \\ &= u_i]_P + \epsilon\phi_i]_P + \epsilon\rho\left(\frac{\partial u_i}{\partial n}\right)_P + O(\epsilon^2). \end{aligned} \tag{8}$$

Since the velocities satisfy the no-slip condition on Γ_M (i.e. $u_i^\epsilon]_{P_\epsilon} = u_i]_P = 0$),

$$\phi_i = -\rho\left(\frac{\partial u_i}{\partial n}\right) \quad \text{on} \quad \Gamma_{\mathrm{M}}. \tag{9}$$

The case of $\epsilon\rho(s)$ negative also yields the same expression. In this case, however, the Taylor series expansion is performed for u_i, since u_i^ϵ is not defined beyond $\Gamma_{\mathrm{M},\epsilon}$ whereas u_i is defined in the region of interest.

The first variation of the objective function is obtained next. The value of the objective function for the new domain is given by,

$$J(\Gamma_{\mathrm{M},\epsilon}) = \int_{\Gamma_{\mathrm{I}}} p^\epsilon u_i^\epsilon n_i \,\mathrm{d}s + \int_{\Gamma_{\mathrm{O}}} p^\epsilon u_i^\epsilon n_i \,\mathrm{d}s. \tag{10}$$

The first variation of the objective function, δJ, is defined by the relation

$$J(\Gamma_{\mathrm{M},\epsilon}) - J(\Gamma_{\mathrm{M}}) = \epsilon\delta J + O(\epsilon^2), \tag{11}$$

and can be shown to be

$$\delta J = \int_{\Gamma_{\mathrm{I}}} \pi u_i n_i \,\mathrm{d}s + \int_{\Gamma_{\mathrm{O}}} \pi u_i n_i \,\mathrm{d}s, \tag{12}$$

which is an integral expression over the entrance and exit boundaries. In the above equation, variation in the objective function due to variation of the exit boundary does not appear since this is a second-order variation in terms of ϵ, the perturbation parameter.

The next step is the transformation of this integral from one that is over Γ_{I} and Γ_{O} to one that is over Γ_{M}. This is achieved through the introduction of an adjoint variable problem. The adjoint problem consists of a set of partial differential equations and boundary conditions and is derived below. Since $u_i n_i$ vanishes on the walls and at the centreline, (12) can be written as

$$\delta J = \oint \pi u_i n_i \,\mathrm{d}s. \tag{13}$$

The inner product of the perturbation equations (6) and the adjoint variables, (z_i, r), integrated over the domain, and added to (13), gives

$$\delta J = \oint \pi u_i n_i \,\mathrm{d}s + \iint r\phi_{i,i} \,\mathrm{d}A + \iint z_i(\nu\phi_{i,jj} - u_j\phi_{i,j} - \phi_j u_{i,j} - \pi_{,i}) \,\mathrm{d}A. \tag{14}$$

The above expression can be rewritten using the divergence theorem as

$$\delta J = \oint \pi(u_i - z_i)\, n_i \, \mathrm{d}s + \nu \oint \left(z_i \frac{\partial \phi_i}{\partial n} - \phi \frac{\partial z_i}{\partial n} \right) \mathrm{d}s$$
$$+ \oint (r\phi_i n_i - \phi_i z_i u_j n_j - u_i z_i \phi_j n_j)\, \mathrm{d}s + \iint \pi z_{i,i}\, \mathrm{d}A$$
$$+ \iint \phi_i (\nu z_{i,jj} + u_j z_{i,j} + u_j z_{j,i} - r_{,i})\, \mathrm{d}A. \tag{15}$$

The adjoint problem has to be defined such that the domain integrals in (15) vanish identically. The choice of boundary conditions for these equations is made such that the only non-zero terms are those that are integrals over Γ_M, the wall that is to be shaped. Let us define the following adjoint problem:

$$\left.\begin{aligned} z_{i,i} &= 0 \quad \text{in} \quad \Omega, \\ \nu z_{i,jj} + u_j (z_{i,j} + z_{j,i}) - r_{,i} &= 0 \quad \text{in} \quad \Omega, \\ z_i &= u_i \quad \text{on} \quad \Gamma. \end{aligned}\right\} \tag{16}$$

Using (7), (9), and (16), (15) can be written as

$$\delta J = \nu \int_{\Gamma_M} \rho(s) \left(\frac{\partial u_i}{\partial n} \right) \left(\frac{\partial z_i}{\partial n} \right) \mathrm{d}s + \nu \int_{\Gamma_I + \Gamma_O} z_i \frac{\partial \phi_i}{\partial n} - \nu \int_{\Gamma_M} r\rho(s) \left(\frac{\partial u_i}{\partial n} \right) n_i \, \mathrm{d}s. \tag{17}$$

The last term on the right-hand side of (17) vanishes since $(\partial u_i/\partial n) n_i$ is identically zero on Γ_M. The integrand of the second term on the right-hand side of (17) is

$$z_i \frac{\partial \phi_i}{\partial n} = z_1 \frac{\partial \phi_1}{\partial n} + z_2 \frac{\partial \phi_2}{\partial n}.$$

This integrand also vanishes, because $z_2 = u_2 = 0$ and $\partial \phi_1 / \partial n = 0$ at the entrance and exit. Notice that $\phi_2 = 0$ at the entrance and exit, therefore $\phi_{1,1} = -\phi_{2,2} = 0$ at Γ_I and Γ_O. Hence (17) is reduced to

$$\delta J = \nu \int_{\Gamma_M} \rho(s) \left(\frac{\partial u_i}{\partial n} \right) \left(\frac{\partial z_i}{\partial n} \right) \mathrm{d}s. \tag{18}$$

In the above equation, the integration is over the boundary that is to be shaped. We can choose $\rho(s)$ as

$$\rho(s) = \omega(s) \left(\frac{\partial u_i}{\partial n} \right) \left(\frac{\partial z_i}{\partial n} \right) \tag{19}$$

since that would ensure a positive change in the objective function, J, for a sufficiently small non-negative weighting function, $\omega(s)$. The function $\rho(s)$ provides the boundary movement for a positive change in J. To evaluate $\rho(s)$ we need to solve the direct problem (i.e. Navier–Stokes equations) given by (1) and (2), and the adjoint problem in z_i given by (16). Note that the optimality condition is satisfied when either the shear stress, $\partial u_i / \partial n$, or the adjoint shear stress, $\partial z_i / \partial n$, on the walls vanishes. The former criterion for optimum diffuser profiles was also pointed out by Chang (1976).

It will be shown that the above formulation is equivalent to the earlier work of

Glowinski & Pironneau (1975). By a change of variable, the adjoint problem can be transformed into the following form:

$$\left.\begin{aligned} w_{i,i} &= 0 && \text{in } \Omega,\\ \nu w_{i,jj}+u_j w_{i,j}-w_j u_{j,i}-q_{,i} &= -u_j u_{i,j} && \text{in } \Omega,\\ w_i &= 0 && \text{on } \Gamma, \end{aligned}\right\} \tag{20}$$

where $2w_i = (z_i - u_i)$ and $2q = (r - p^* + \frac{1}{2}u_j^2 - u_j z_j)$. The first variation of the objective function then becomes

$$\delta J = \nu \int_{\Gamma_M} \rho \left(\frac{\partial u_i}{\partial n}\right)\left(\frac{\partial u_i}{\partial n} + 2\frac{\partial w_i}{\partial n}\right) \mathrm{d}s. \tag{21}$$

The form of the adjoint variable problem defined by (20) is identical to that derived by Glowinski & Pironneau (1975). Either one of the above adjoint problems can be solved numerically to obtain the next shape. However upon examination of (20), it becomes evident that the $w_j u_{j,i}$ term may lead to a numerically unstable scheme. This is because the approach to steady state would be attained via an iterative 'time evolution'-like scheme that would then be of the form $\mathrm{d}w/\mathrm{d}t = w(\text{const}) + \ldots$. This form is likely to result in the exponential growth of the inevitable roundoff and truncation errors present at any iterative step. Also the presence of the inhomogeneous term, $-u_j u_{i,j}$, in the above equations may lead to a linear growth of the roundoff and truncation errors in the numerical computations.

It is expected that these numerical difficulties will be absent in the (z_i, r) formulation of the adjoint variable problem obtained in this paper and given by (16). Hence this is the set of equations for which the algorithm for the numerical solution of the adjoint problem is developed.

As pointed out by Pironneau (1974), the adjoint equations do not seem to arise from any identifiable physical phenomenon. It is however possible to demonstrate that the adjoint variable problem is associated with a certain artificially constructed flow. A change of variables leads to the following form:

$$\left.\begin{aligned} z'_{i,i} &= 0 && \text{in } \Omega,\\ \nu z'_{i,jj} - u'_j(z'_{i,j}+z'_{j,i}) - r'_{,i} &= 0 && \text{in } \Omega,\\ z'_i = u'_i &= -u_i && \text{on } \Gamma, \end{aligned}\right\} \tag{22}$$

where $z'_i = -z_i, u'_i = -u_i$, and $r' = -r$. The first equation in (22) is identical to the continuity equation. Compare the second equation in (22) with the Navier–Stokes equation written here in a slightly different form:

$$\nu u_{i,jj} - u_j(u_{i,j}+u_{j,i}) - \tilde{p}_{,i} = 0, \tag{23}$$

where $\tilde{p} = p^* - \frac{1}{2}u_k^2$. Observe that the problem in the adjoint variable z'_i is analogous to the Navier–Stokes problem in the variable u_i with the following exception: the convective velocities in the adjoint problem are specified, rendering the problem linear, and are obtained from the direct problem. These convective velocities, u'_i, are identical in magnitude but opposite in direction to those of the 'direct' problem. The boundary conditions for the adjoint variables are $z'_i = -u_i$ on Γ. Hence on the walls they imply a no-slip condition as in the direct problem. But at the inflow and outflow boundaries, 'adjoint' flow is found entering at the domain exit Γ_O and leaving at the domain entrance Γ_I, thus suggesting an 'adjoint' flow in the direction opposite to that of the actual flow.

The above interpretation of the adjoint variable problem will be useful in constructing a modified problem whose solution will provide numerical values, albeit

approximate, for the shear stress, $\partial u_i/\partial n$, and the adjoint shear stress, $\partial z_i/\partial n$, in (19). It is found that a shape optimization algorithm that obtains its boundary movement from these approximate numerical solutions does indeed lead to diffuser shapes that satisfy the optimality condition.

4. Numerical aspects

The theoretical results obtained above are not limited to diffusers alone but are in fact valid for the optimal design of any internal flow component with boundary conditions in (2) and the objective function of (3). With these same boundary conditions and objective function the analysis can be extended to three-dimensional flows as well leading to a result similar to that in (19). The above analysis requires both the inflow and the outflow boundary condition to be of the Dirichlet type. While Dirichlet-type conditions are likely to be known at inflow, the same is not true in practice at outflow, except under special circumstances. For example for finite-sized ducts one would be limited to the case of fully developed flow throughout the duct, leading to a constant-area duct, not a geometry of particular interest here. For ducts and channels of varying cross-section where fully developed flow may exist at the entrance but not at the exit, one would require a downstream extension long enough to permit the establishment of fully developed flow. The length of such a downstream extension is not known *a priori* and may be so large as to render a numerical approach intractable. On the other hand if the length of the component is truncated to preclude established flow at the exit, *a priori* knowledge of Dirichlet conditions at the exit is impossible. Even if such a downstream Dirichlet condition were available, Kreiss & Lorenz (1989) remark that Neumann conditions at outflow lead to a 'smoother' solution. Such a solution would then be more readily amenable to numerical treatment. Hirsch (1990) also suggests the use of Neumann-type outflow conditions provided one can ensure that there is no flow reversal anywhere on the outflow boundary. Thus it would be desirable to carry out the same analysis as above but replacing the outflow Dirichlet conditions with the less restrictive Neumann conditions. We failed to derive the adjoint problem for this choice however because the domain integrals in (15) do not drop out as they do in the present analysis. It is therefore instructive to determine whether the theoretical result with Dirichlet outflow conditions continues to hold even if the direct as well as the adjoint solutions are carried out with Neumann-type outflow conditions instead. Lacking formal proof, we resort to *a posteriori* justification of this postulate, a discussion of which appears in §5 along with the results. Finally it is shown that the computed 'optimal' shapes do indeed satisfy the optimality condition that follows from (18).

4.1. *Boundary conditions for Navier–Stokes equations*

A parallel flow assumption at the upstream boundary implies Dirichlet boundary conditions for both the velocity components. Instead, a computationally desirable Neumann condition for the transverse velocity component ($\partial u_2/\partial n = 0$ on Γ_1) is substituted while retaining a Dirichlet condition for the streamwise component. A parabolic profile corresponding to a fully developed laminar flow is specified for this component. At the downstream boundary the parallel flow assumption is replaced with computationally desirable Neumann conditions for both the velocity components ($\partial u_1/\partial n = \partial u_2/\partial n = 0$ on Γ_0). Similar approximations will be made in the solution of the adjoint variable problem, keeping in mind the reversal of the role of entrance and exit boundaries. At the solid wall, a boundary whose profile is to be

determined, a no-slip condition is enforced. At the diffuser centreline the usual symmetry conditions are used since the flow is assumed to be symmetric. The complete set of velocity boundary conditions utilized in obtaining the numerical solution to the direct problem is therefore given by

$$\left.\begin{aligned}
\frac{u_1}{V} &= \frac{3}{2}\left[1-4\left(\frac{y}{W_1}\right)^2\right] \quad \text{on} \quad \Gamma_{\mathrm{I}},\\
\frac{\partial u_2}{\partial n} &= 0 \quad \text{on} \quad \Gamma_{\mathrm{I}},\\
\frac{\partial u_i}{\partial n} &= 0 \quad \text{on} \quad \Gamma_{\mathrm{O}} \quad (i=1,2),\\
u_i &= 0 \quad \text{on} \quad \Gamma_{\mathrm{M}} \quad (i=1,2),\\
\frac{\partial u_1}{\partial n} &= 0 \quad \text{on} \quad \Gamma_{\mathrm{C}},\\
u_2 &= 0 \quad \text{on} \quad \Gamma_{\mathrm{C}}.
\end{aligned}\right\} \tag{24}$$

At the entrance, exit, and wall, pressure has been extrapolated from within the domain by assuming that the second derivative of the pressure vanishes on the domain boundary. At the centreline a symmetry condition is imposed in the numerical scheme for the pressure.

4.2. *Boundary conditions for adjoint equations*

The roles of entrance and exit are reversed for the adjoint equations. Therefore, at the exit boundary a Dirichlet-type condition is used only for the streamwise component of the co-state vector. Therefore we set $z_1 = u_1$ on Γ_{O}, with u_1 taken from the solution of the Navier–Stokes equations. For the remaining component z_2 of the co-state vector at the exit and for both components of the co-state vector at the entrance, Neumann conditions are employed instead. At the wall where all velocity components vanish and, therefore, z_i the co-state vector that is analogous to the velocity is set to zero. The adjoint variable, r^*, is analogous to the pressure term in the Navier–Stokes equations and hence no analytical boundary condition is available for this variable. However, a computational boundary condition is implemented for this variable. The value of r^* is extrapolated to the boundary from values at interior points assuming that the streamwise second derivative vanishes at the boundary. This is done at all boundaries except at the centreline where a symmetry condition is enforced. Therefore the numerical solution to the adjoint problem is obtained for the following set of boundary conditions:

$$\left.\begin{aligned}
\frac{\partial z_i}{\partial n} &= 0 \quad \text{on} \quad \Gamma_1 \quad (i=1,2),\\
z_1 &= u_i \quad \text{on} \quad \Gamma_{\mathrm{O}},\\
\frac{\partial z_2}{\partial n} &= 0 \quad \text{on} \quad \Gamma_{\mathrm{O}},\\
z_i &= 0 \quad \text{on} \quad \Gamma_{\mathrm{m}} \quad (i=1,2),\\
\frac{\partial z_1}{\partial n} &= 0 \quad \text{on} \quad \Gamma_{\mathrm{C}},\\
z_2 &= 0 \quad \text{on} \quad \Gamma_{\mathrm{C}}.
\end{aligned}\right\} \tag{25}$$

5. Numerical solvers

5.1. *Navier–Stokes equations solver*

The primitive variable form of the incompressible steady Navier–Stokes equations is solved using a finite volume formulation. One of the main difficulties associated with the solution of the Navier–Stokes equations in the velocity–pressure formulation is the imposition of continuity, which must be satisfied at all times. This does not permit the use of a simple explicit method that avoids solution of an algebraic system of equations at each time step. If only steady-state solutions are of interest, Chorin (1967) has shown that this difficulty can be overcome by use of an artificial compressibility method. In this formulation, the continuity equation is modified using the time derivative of the pressure term. Together with the unsteady momentum equations, this forms a hyperbolic-parabolic type of time-dependent system of equations. The steady-state solution of the Navier–Stokes equations is then obtained as the large-time solution of the unsteady momentum equations with the perturbed divergence equation. These unsteady equations are

$$\left.\begin{aligned} p_t^* + \beta^2 u_{i,i} &= 0, \\ u_{i,t} + (u_j u_i)_{,j} &= -p_{,i}^* + \nu u_{i,jj}, \end{aligned}\right\} \tag{26}$$

where β is analogous to the speed of sound. Note that these equations do not represent any transient physical phenomenon and hence the transient solution has no physical meaning until steady state is attained. This is indicated by the vanishing of the time-derivative terms in the numerical solution.

The equations are normalized using the velocity and length scales V and W_1 defined earlier. In addition time and pressure are normalized using the ratio W_1/V and ρV^2 respectively. The Reynolds number of the flow through the diffuser is then given by $Re = (VW_1)/\nu$.

The equations are discretized in space using a finite-volume formulation. The spatial discretization is performed on the conservative form of the governing equations using a central-difference scheme. The physical domain is divided using a computational grid consisting of nearly orthogonal cells. For the cells in the interior of the domain, the dependent variables are evaluated at the cell centre. For the cells on the domain boundary, the dependent variables are evaluated at the cell face adjoining the boundary. The main advantage of the finite-volume formulation is that an irregular physical domain is mapped onto a regular computational domain.

An explicit one-step multistage Runge–Kutta stepping scheme is used for integration in time. While implicit scheme have less restrictive stability requirements, explicit scheme are easier to code and vectorize. The use of an explicit Runge–Kutta method as a time-stepping scheme for the solution of the compressible Euler equations has become popular following the work of Jameson, Schmidt & Turkel (1981) and Rizzi & Eriksson (1984). This approach has been extended to the compressible Navier–Stokes equations by Swanson & Turkel (1985) and Vatsa (1986). Further extensions to incompressible flow have been made by Rizzi & Eriksson (1985) and to incompressible turbulent flow by Sung (1987).

Use of a Runge–Kutta method relaxes the severe time-step restriction of the conventional explicit methods by enlarging the stability region. Since transient behaviour is not an issue and a larger time step is desirable, a four-stage Runge–Kutta scheme with first-order accuracy in time and a relatively high Courant–Friedrichs–Lewy number has been chosen. In order to improve the convergence rate,

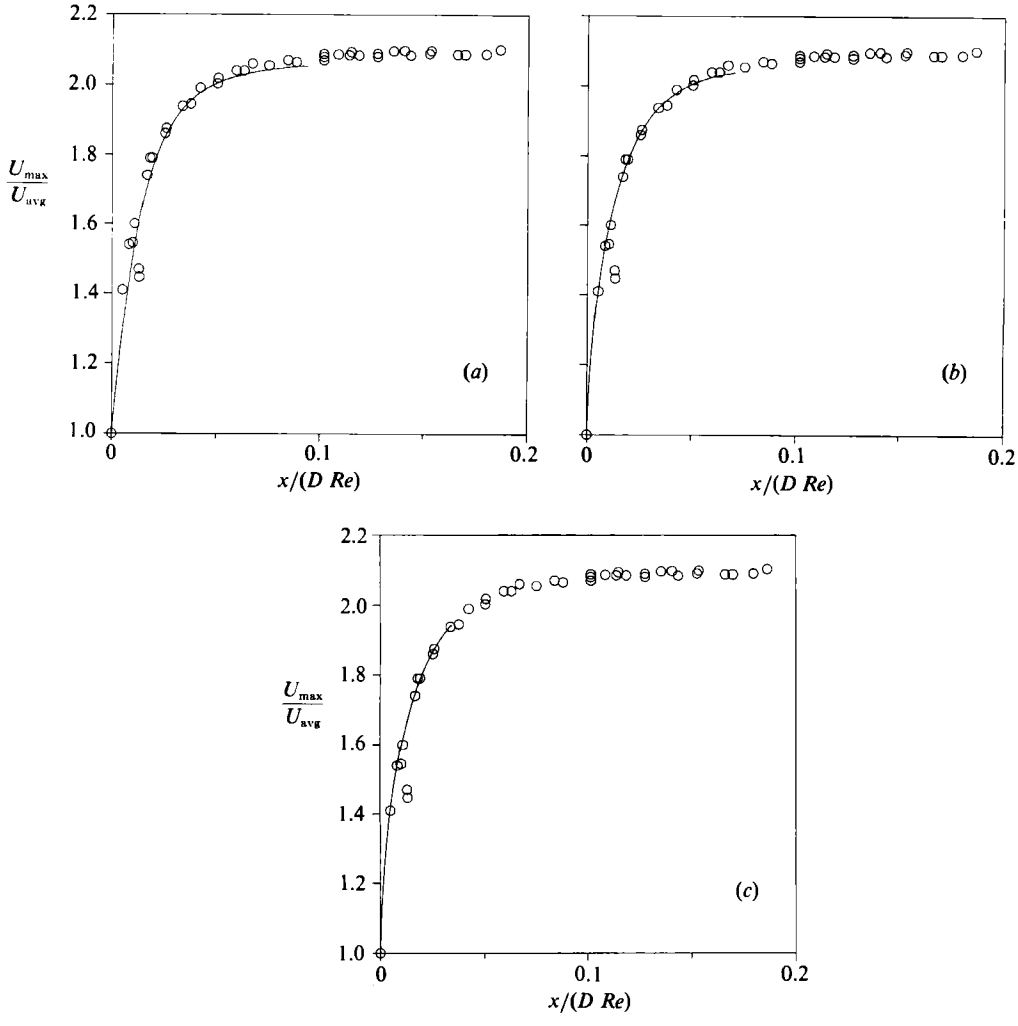

FIGURE 2. Streamwise velocity development along the duct centreline: (*a*) $Re = 32$, (*b*) $Re = 100$ and (*c*) $Re = 100$ (shorter computational domain). ——, Computations; ○, Goldstein & Kreid (1967).

a local time step is computed for each cell at each elapsed time level. These time steps have been estimated from a stability analysis of the algorithm. A fourth-order linear artificial dissipation term is introduced to damp the high-frequency oscillations associated with the so-called sawtooth or plus-minus waves, i.e. waves associated with the shortest wavelengths. Implicit residual smoothing is performed at each iteration to enhance the stability region of the technique.

5.2. *Test solutions of the Navier–Stokes solver*

To establish some measure of confidence in the numerical solution of the Navier–Stokes equations the three-dimensional version of the code was used to compute entry flow in a straight duct of square cross-section at $Re = 32$ and 100. The Reynolds number is based on the average velocity through the duct and the duct width. The calculations are carried out in a single quadrant of the duct, owing to symmetry.

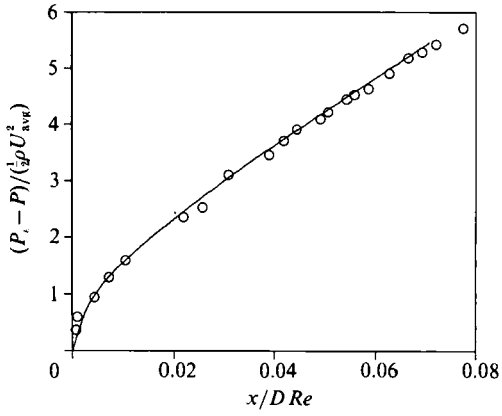

FIGURE 3. Variation of the average pressure with $x/(DRe)$ at $Re = 100$. ——, Computations; ○, Beavers *et al.* (1970).

The number of grid points in the streamwise, i.e. x, direction varies from 17 at $Re = 32$ to 52 at $Re = 100$ with a 9×9 grid in the other, i.e. y- and z-directions. The grid spacing is somewhat non-uniform in the x-direction close to the duct entrance but is uniform in the other two directions. At the entrance a plug flow profile is specified for the streamwise velocity component and the streamwise derivative of the remaining velocity components is set to zero. At the exit the streamwise derivative is assumed to vanish for all three velocity components. The usual no-slip condition on the wall and symmetry conditions at the two centreplanes are specified.

Figures 2(*a*), 2(*b*) and 2(*c*) show the axial development of the computed as well as the measured normalized streamwise velocity component at the duct centreline. Figures 2(*a*) and 2(*b*) show the calculations at Reynolds numbers of 32 and 100 respectively, whereas figure 2(*c*) shows the calculation at a Reynolds number of 100 but for a computational domain shorter than that used for figure 2(*b*). The experimental data were obtained from the laser Doppler velocimetry measurements of Goldstein & Kreid (1967) for Reynolds numbers ranging between 69 and 387. As seen from these figures, the calculations agree with the experimental data. The shorter-domain results shown in figure 2(*c*) do not differ from the results in figure 2(*b*), indicating the efficacy of Neumann-type downstream boundary conditions in minimizing the upstream influence on the flow. In figure 3 the computed pressure averaged over the cross-sectional area is compared with the experimental data of Beavers, Sparrow & Magnuson (1970) at $Re = 100$. Once again the agreement between calculations and the experimental data is found satisfactory. The above test-case results provide a measure of confidence in the ability of the code to accurately model the boundary-layer development in the entrance region of the duct.

5.3. *Mesh generation*

The computational grid is generated by solving a set of elliptic partial differential equations similar to those suggested by Thompson, Thames & Mastin (1974). They begin with the following coordinate mapping:

$$\left.\begin{aligned} \alpha x_{\xi\xi} - 2\beta x_{\xi\eta} + \gamma x_{\eta\eta} &= 0, \\ \alpha y_{\xi\xi} - 2\beta y_{\xi\eta} + \gamma y_{\eta\eta} &= 0, \end{aligned}\right\} \tag{27}$$

where $$\alpha = x_\eta^2 + y_\eta^2, \quad \beta = x_\xi x_\eta + y_\xi y_\eta, \quad \gamma = x_\xi^2 + y_\xi^2.$$

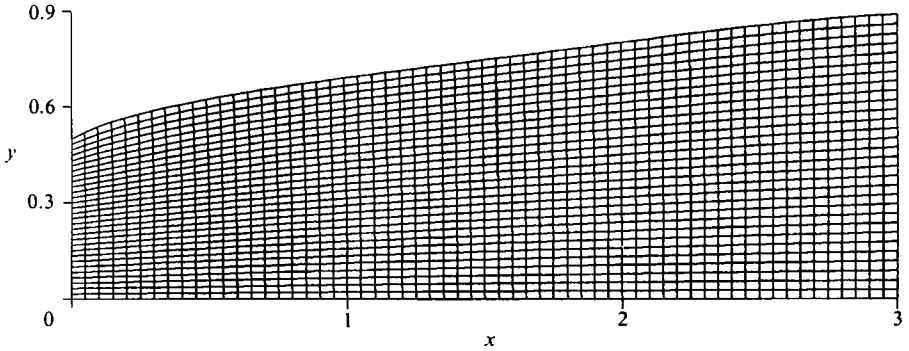

FIGURE 4. A typical computational grid for a plane diffuser obtained using the grid generation program. Grid size is 61×31. This was the domain for the optimum diffuser at $Re = 200$ and $L/W_1 = 3$.

In this paper, the above equations are simplified by assuming that $\alpha \approx \gamma$ and $\beta \approx 0$, and instead the following equations are solved:

$$\left.\begin{aligned} x_{\xi\xi} + x_{\eta\eta} &= 0, \\ y_{\xi\xi} + y_{\eta\eta} &= 0, \end{aligned}\right\} \tag{28}$$

in the computational domain, $1 < \xi < \xi_{\max}$ and $1 < \eta < \eta_{\max}$, with Dirichlet boundary conditions.

The equations are discretized using finite differences. The set of algebraic equations thus obtained is solved by successive over-relaxation. The grids generated using this method have been found to be satisfactory for the purposes of this paper. A typical grid is shown in figure 4. Grids generated by this method were nearly orthogonal and the cell dimensions in each direction are approximately equal.

5.4. *Adjoint equation solver*

The solution to the adjoint set of equations is obtained as the steady-state solution to the following set of equations:

$$\left.\begin{aligned} r_t^* &= -\beta^2 z_{i,i}, \\ z_{i,t} &= \nu z_{i,jj} + u_j(z_{i,j} + z_{j,i}) - \tfrac{1}{2}(z_k z_k)_{,i} - r_{,t}^*, \end{aligned}\right\} \tag{29}$$

where $r^* = r - \frac{1}{2} z_k z_k$. A nonlinear term $\frac{1}{2}(z_k z_k)_{,i}$ is introduced in the above equation to enhance the rate of convergence. The utility of this term was established by means of preliminary calculations performed on a straight-duct geometry where an exact solution of the Navier–Stokes solution is known for fully developed laminar flow.

The equations are normalized following a procedure similar to that utilized for the Navier–Stokes equations. The non-dimensional form of (29) is identical to the dimensional one with the exception of the first term on the right-hand side where the kinematic viscosity, ν, is replaced by the reciprocal of the Reynolds number.

The numerical algorithm for the solution of the adjoint set of equations is essentially similar to the algorithm described for the Navier–Stokes equations. Some subtle but important differences do exist since the equations solved are after all not the same. A brief discussion of the numerical algorithm is presented here, since this solution, to the best of our knowledge, represents the first successful numerical solution of the adjoint set of equations in the absence of either a thin boundary layer

or a Stokes flow assumption. Spatial discretization is carried out by a centred-different finite-volume formulation. The term $u_j(z_{i,j}+z_{j,i})$ on the right-hand side of (29) is not in a divergence form. In the treatment of this term the velocities u_j, which have already been obtained by the Navier–Stokes solver, are treated as known quantities and are assumed constant inside each cell. Hence the volume integral over the cell is performed by applying the divergence theorem to the remaining part of this term, i.e. $(z_{i,j}+z_{j,i})$.

The other terms in (29) are treated in the same fashion as the finite-volume formulation of the Navier–Stokes equations. Once again a fourth-order linear artificial dissipation term is introduced to damp high-frequency oscillations. Time integration is carried out by a Runge–Kutta scheme with local time stepping. Implicit residual smoothing has also been incorporated into the scheme. The details and a thorough verification of the numerical schemes for both the Navier–Stokes and the adjoint set of equations are given by Çabuk (1991).

5.5. *Profile modification algorithm*

The principal steps of the optimization procedure are:

(*a*) choose an initial diffuser profile;

(*b*) generate a computational grid that conforms to the diffuser wall;

(*c*) obtain the steady-state solution to the direct problem;

(*d*) obtain the steady-state solution to the adjoint problem, by treating the required velocities as known from step (*c*);

(*e*) compute $\partial u_i/\partial n$ and $\partial z_i/\partial n$ from the solutions in steps (*c*) and (*d*) respectively. Choose a non-negative weighting function $\omega(s)$ and hence obtain $\rho(s)$ from (19);

(*f*) move nodes on the diffuser wall to be profiled along the outer normal direction by $\rho(s)$. The curve connecting the nodes after this movement represents the new diffuser profile;

(*g*) go to step (*b*) unless the change in diffuser pressure rise obtained from step (*c*) is smaller than a desired convergence parameter.

The iterative profile modification process is continued until the change in pressure rise is a small fraction of the total pressure rise. An alternative method is to continue the process until the value of $\rho(s)$ everywhere along the wall is less than a critical value.

In step (*e*), the weighting function, $\omega(s)$, is chosen to be proportional to the arclength, s, along the diffuser wall measured from the diffuser entrance. This ensures that the entrance width is maintained constant but the exit width may vary with the diffuser profile.

When shifting the diffuser wall profile to a new curve obtained from step (*f*) some care must be exercised since the curve is being redefined using only a finite number of discretely spaced points. Some checks are performed on the location of points on the new curve and the following heuristic measures are adopted. (i) A means to ensure that boundary nodes do not conglomerate or coalesce after their movement to a new position so as to prevent degradation of numerical accuracy elsewhere in the domain where points are now spaced far apart. (ii) A means to ensure that the appearance of small-amplitude wiggles in the new profile are damped to some extent so as to prevent the growth and build-up of numerical errors in the subsequent calculation.

In order to prevent the points on the wall boundary from coalescing, these points are moved tangentially after their prescribed normal movement so that the spacing between them remain approximately equal (see figure 5). In figure 5, line l_1 is parallel

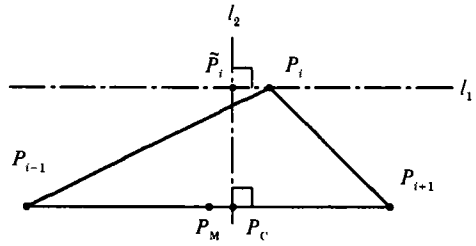

FIGURE 5. Schematic diagram for the tangential relocation of the boundary points. $P_C = P_M + \beta\{|\kappa_i + 1| - |\kappa_i - 1|\}$, P_M is the midpoint of $\overline{P_{i-1}P_{i+1}}$.

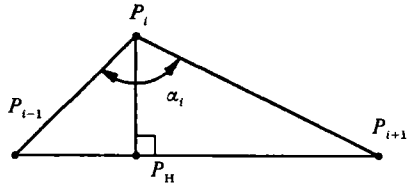

FIGURE 6. Schematic diagram for reduction of corner angles.

to $\overline{P_{i-1}P_{i+1}}$ and passes through point P_i, and line l_2 is perpendicular to the line l_1 and passes through the point P_C on $\overline{P_{i-1}P_{i+1}}$. In order to maintain even spacing, P_C should correspond to the midpoint P_M of $\overline{P_{i-1}P_{i+1}}$. However, an actual curve is better represented by a collection of node points, if the density of the nodes increases with the absolute value of the curvature along the curve. In order to get relatively smaller spacing when the absolute value of the curvature is large, the point P_C is computed as follows. The midpoint P_M of $\overline{P_{i-1}P_{i+1}}$, and $|\kappa_{i-1}|$ and $|\kappa_{i+1}|$, the absolute values of curvatures at P_{i-1} and P_{i+1} respectively, are computed. Then P_C is found from $P_C = P_M + \beta(|\kappa_{i+1}| - |\kappa_{i-1}|)$ where β is a weighting factor. Point $\tilde{P}_i$ is the intersection of line l_1 and line l_2. For each node on Γ_M, points $\tilde{P}_i$ are computed first, then the P_i are replaced by $\tilde{P}_i$. This tangential relocation of the node points assures that they will not coalesce. Furthermore, a tangential relocation of nodes does not change the value of the objective function, J, considerably since the curve defining the relocated nodes is essentially the same as before relocation.

The wall boundary points are also relocated to damp the occurrence of wiggles in the new profile. Boundary points are moved as shown in figure 6, if the deviation of the corner angles from π was more than a pre-specified angle, in such a way as to ensure that this deviation would be less than or equal to the specified tolerance. The corner angles, α_i, in figure 6 are computed for all nodes on Γ_M. If $\max|\alpha_i - \pi|$ is greater than a preset threshold of $\frac{1}{4}\pi$, the corresponding point, P_i, is moved to the midpoint of $\overline{P_i P_H}$. This process is continued until $\max|\alpha_i - \pi|$ is less than the threshold. This relocation procedure assures that the new profile at any iteration is sufficiently free of very sharp corners.

6. Results and discussion

Using the numerical solvers and the profile modification algorithm described above, optimum diffuser profiles have been obtained for a single diffuser length $L/W_1 = 3$ at Reynolds numbers $Re = 50$, 100, 200 and 500. A sound speed, β^2, of 2 for the Navier–Stokes equations and 2.5 for the adjoint equations was used at all Reynolds numbers. The calculation at $Re = 200$ (henceforth called the reference case) has been examined in particular detail to establish issues of convergence and accuracy.

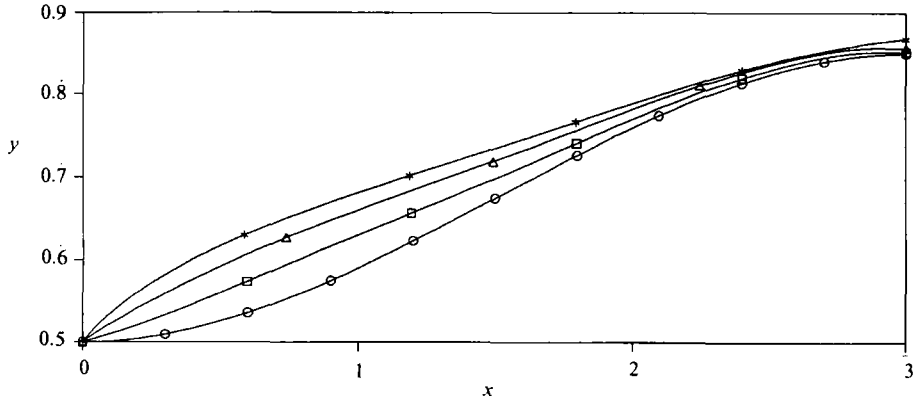

FIGURE 7. Profiles of a reference diffuser at successive iterations. The grid size is 61×31. ○, Initial shape; □, first iteration; △, fourth iteration; *, ninth iteration.

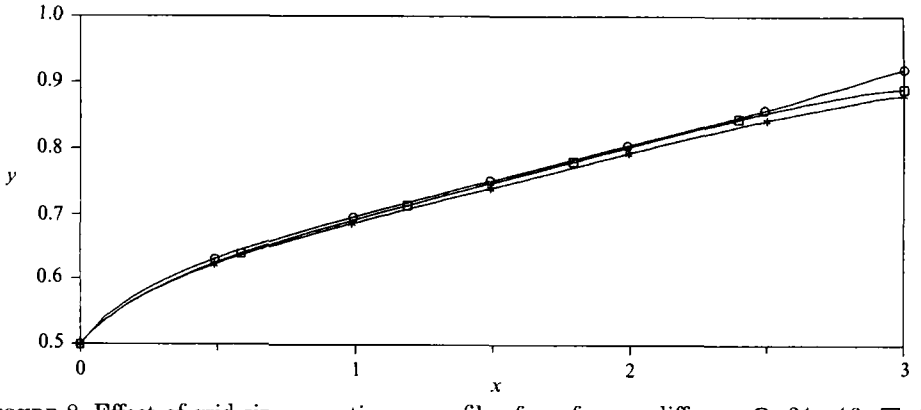

FIGURE 8. Effect of grid size on optimum profile of a reference diffuser: ○, 31×16; □, 61×31; *, 121×61.

The reference case was first examined for convergence of the profile modification algorithm. For this purpose, a computational grid of 61 nodes in the x- and 31 nodes in the y-directions is employed, both for the Navier–Stokes and the adjoint variable problem. Beginning with an initial shape, the diffuser profile was obtained after each application of the shape modification algorithm. The initial profile and some of the intermediate profiles are shown in figure 7. The change in the profile shape is observed to be small between the fourth and the ninth iteration and the change was found to be insignificant after nine iterations. Hence the iterative process is stopped at the ninth iteration, providing a reasonably converged optimum shape. The question of computational accuracy of the solvers and hence the accuracy of the optimum profile is addressed next.

The precise error due to a finite grid size on the optimum profile is difficult to determine since the actual optimum curve is not known *a priori*, nor are any other calculations or experimental data available. However one way to estimate the effects of the unavoidable truncation errors in a numerical calculation is to obtain the optimum diffuser profile using progressively finer grids until there is no change with grid size. Once again the reference case of $Re = 200$ was examined for this purpose using grids of 31×16, 61×31 and finally 121×61. The optimum profiles obtained using the three grids are shown in figure 8. The results show that the difference between the shapes is negligibly small, providing some evidence that at these grids

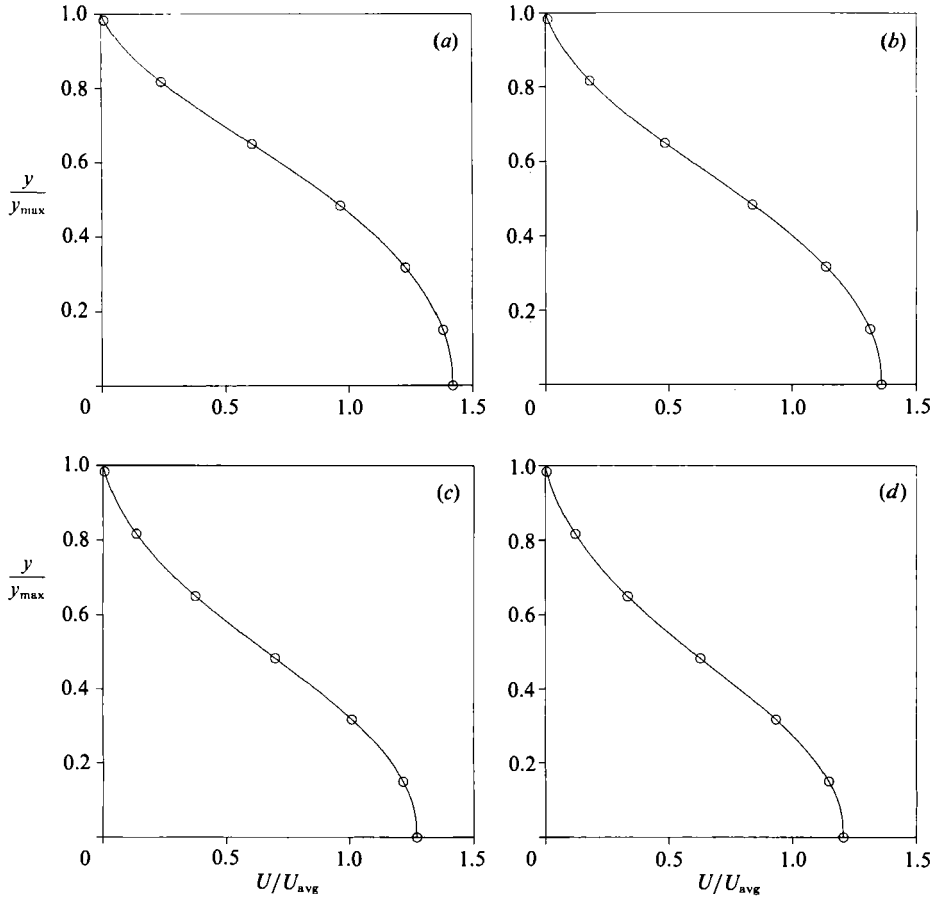

FIGURE 9. Development of the streamwise velocity profile along the reference diffuser. The grid size is 61×31. (*a*) $x = 0.5$, (*b*) $x = 1.0$, (*c*) $x = 2.0$, and (*d*) $x = 3.0$.

the contribution of the truncation errors may not be significant. In view of this observation, a grid size of 61×31 is found to be a suitable compromise between accuracy and computational work for the results presented here.

In an earlier section we proposed that it was computationally desirable to impose Neumann-type conditions at outflow boundaries in both the Navier–Stokes and the adjoint equation solvers. To justify this postulate we need to verify whether the optimum shapes obtained in this fashion do indeed satisfy the optimality condition, i.e. vanishing shear stress on the wall, arising from the analysis. The velocity profiles and wall shear stress for the optimum reference diffuser are examined for this purpose. In figure 9, the streamwise velocity distribution across the diffuser is shown at several axial positions. The slope of the velocity profile is observed to approach zero as the wall is approached, i.e. $y = y_{\max}$ of the optimum diffuser. In figure 10 the wall shear stress normalized by the corresponding value for a straight duct is shown for the optimum shape as well as at several intermediate stages of iteration. The wall shear stress for the optimum shape is found to be vanishingly small for all but 10% of the wall at the upstream end. The shear stress distributions at intermediate iterations demonstrate a monotonic decrease towards the optimum values. Closer examination of the shear stress for the optimum and intermediate shapes at other Reynolds numbers confirm the same behaviour. To eliminate the possibility that the

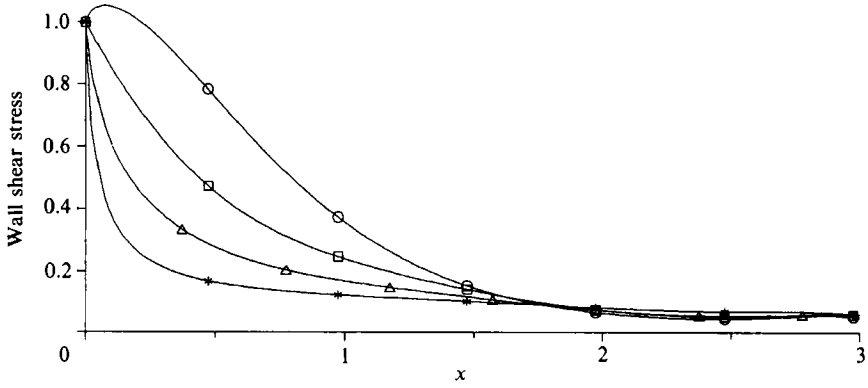

FIGURE 10. Normalized wall shear stress at successive iterations for a reference diffuser. The grid size is 61×31. ○, Starting shape; □, first iteration; △, fourth iteration; *, ninth iteration.

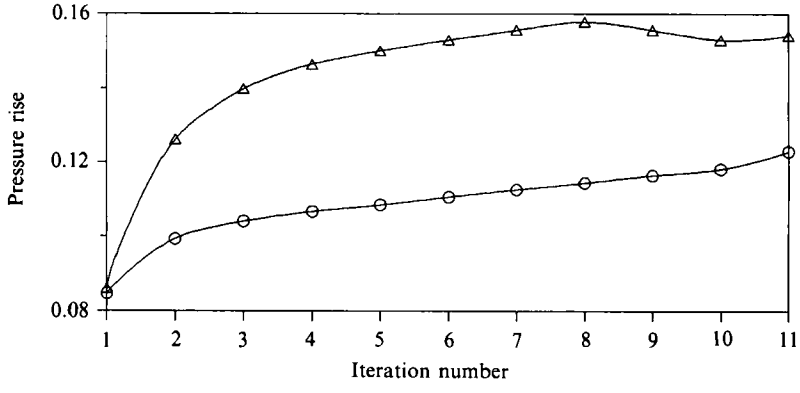

FIGURE 11. Static pressure rise through the reference diffuser at successive iterations. The grid size is 61×31. ○, Area-averaged pressure rise; △, velocity-averaged pressure rise.

approach to optimum is in some sense non-systematic due to the postulated Neumann-type outflow conditions, we examine the iterative history of the objective function for the reference diffuser. The velocity-averaged static pressure rise (i.e. the objective function defined by (3)) is shown in figure 11 at successive iterations of the shape modification process. The objective function for this modified numerical problem is indeed found to increase with each application of the boundary movement suggested by (19). The area-averaged static pressure rise through the reference diffuser also increases with shape modification, as seen in figure 11. These observations are also valid for calculations at other Reynolds numbers in the present study. The *a posteriori* checks performed on the numerical results hence permit us to place a fair degree of confidence in the validity of the numerical approach.

In addition to the reference case, calculation of the optimum diffuser profile was carried out at three other Reynolds numbers, $Re = 50$, 100 and 500. in figure 12, these profiles are shown for a diffuser of $L/W_1 = 3$ for a grid of 61×31. At lower Reynolds numbers the optimum diffuser profile permits a larger ratio of exit area to inlet area, as one would expect higher viscous effects to support greater diffusion without separation. The angle at which the diffuser profile departs at the upstream corner is difficult to compute accurately since the flow in that corner may not be accurately resolved. Nevertheless, the approximate angle decreases from 56° to 19°

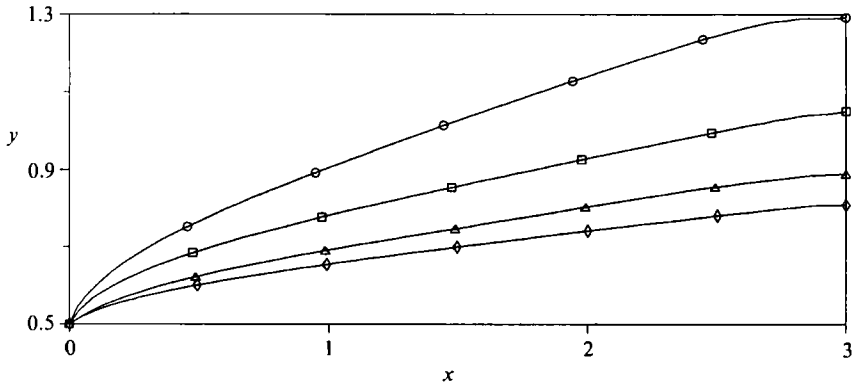

FIGURE 12. Optimum diffuser profiles at different Reynolds numbers for $L/W_1 = 3$. Grid size is 61×31. ○, $Re = 50$; □, $Re = 100$; △, $Re = 200$; ◇, $Re = 500$.

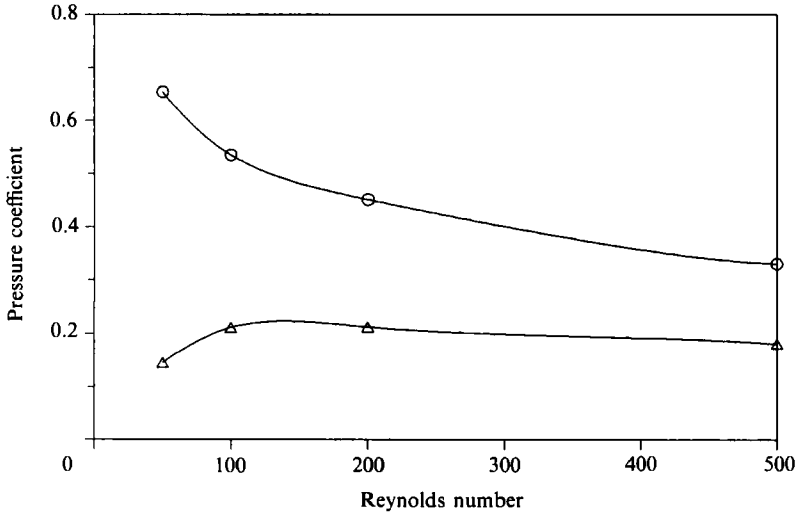

FIGURE 13. Variation of the pressure coefficient, C_p with Reynolds number for $L/W_1 = 3$. ○, Optimal diffusers; △, straight diverging diffusers.

as the Reynolds number increases from 50 to 500. For the Reynolds-number range in which numerical solutions are presented here, further refinement of the grid did not lead to any significant change in the optimum profile. This was not found to be true of computations at Reynolds numbers higher than 500.

To evaluate the performance of the optimum diffuser, a pressure recovery coefficient, C_p, is defined, which is the ratio of the static pressure rise of the optimum diffuser to the static pressure rise for an ideal diffuser (in potential flow) with the same W_2/W_1 ratio as the optimum diffuser. Note that the denominator of this ratio is independent of the actual profile between the upstream and downstream cross-sections of the diffuser. Using C_p as a parameter, the performance of the optimum diffuser is now compared with that of a straight-walled diffuser with the same W_2/W_1 ratio at several different Reynolds numbers in the laminar regime. The C_p values of straight diffusers are found numerically using the Navier–Stokes solver on the straight-walled geometry without any shape modification steps. As seen from figure 13, the C_p values for the optimum diffusers are always higher than those for straight diffusers.

7. Conclusion

A variational formulation of the problem of determining the profile of a plane diffuser (of given upstream width and length) that provides the maximum static pressure rise is derived. The analysis provides a set of 'adjoint' equations, the solution to which along with the solution to the 'direct' Navier–Stokes equations provide a means to compute the direction and relative magnitude of the change in diffuser profile that leads to a higher pressure rise. The optimality condition, that the shear stress all along the wall must vanish for the optimum diffuser, is also recovered from the analysis.

It is shown that the adjoint problem may be associated with an artificially constructed flow. The convective velocities of this problem are identical in magnitude but opposite in direction to those of the direct problem. At the inflow and outflow boundaries, 'adjoint' flow is found entering at the domain exit Γ_O and leaving at the domain entrance Γ_I, thus suggesting an 'adjoint' flow in the direction opposite to that of the actual flow. This interpretation of the adjoint problem is found useful in constructing the numerical solution to the adjoint problem.

The direct as well as the adjoint set of partial differential equations are obtained for Dirichlet-type inflow and outflow conditions. It is postulated that the adjoint set of equations continue to hold even if the computationally inconvenient Dirichlet-type outflow boundary condition is replaced by Neumann-type conditions. Results obtained in this fashion are examined to provide *a posteriori* justification of this postulate. It is shown that numerical solutions obtained in this fashion do satisfy the optimality condition. Future effort should address the inadequate treatment of the outflow boundary condition in obtaining the adjoint problem.

The analysis in its present form can be extended to three-dimensional flow to obtain a shape modification formula similar to that in (18). It however remains to be examined whether the numerical approach continues to hold in more complex geometries where the flow is necessarily three-dimensional, perhaps due to an associated non-negligible secondary flow.

The research reported in this paper is based upon work supported by the National Science Foundation under Grant Numbers CBT-87-10561, ASC-91-10514 and ASC-90-0021P. The authors gratefully acknowledge and thank Dr Chao-Ho Sung of the David Taylor Research Center for his assistance with the development of the computational algorithm. The authors would also like to thank the Referees whose comments and criticism resulted in significant changes and in our opinion improvement in the quality of this paper.

REFERENCES

Beavers, G. S., Sparrow, E M. & Magnuson, R. A. 1970 Experiments on hydrodynamically developing flow in rectangular ducts of arbitrary aspect ratio. *Intl J. Heat Mass Transfer* **13**, 689–701.

Çabuk, H. 1991 *Optimum design in fluid mechanics.* Ph.D. thesis, Columbia University Department of Mechanical Engineering.

Çabuk, H. & Modi, V. 1990 Shape optimization analysis: first- and second-order necessary conditions. *Optimal Control Applics Meth.* **11**, 173–190.

Chang, P. K. 1976 *Control of Flow Separation.* McGraw Hill.

Chorin, A. J. 1967 A numerical method for solving incompressible viscous flow problems. *J. Comput. Phys.* **2**, 12–26.

GARABEDIAN, P. R. & KORN, D. G. 1971 Numerical design of transonic airfoils. In *Proc. SYNSPADE, 1970* (ed. B. Hubbard), pp. 253–271. Academic.

GARABEDIAN, P. & MCFADDEN, G. B. 1982 Computational fluid dynamics of airfoils and wings. In *Proc. Symp. on Transonic, Shock, and Multidimensional Flows, Madison, 1981* (ed. R. Meyer), pp. 1–16. Academic.

GILES, M., DRELA, M. & THOMPKINS, W. T. 1985 Newton solution of direct and inverse transonic Euler equations. *AIAA Paper* 85–1530; *Proc. AIAA 7th Computational Fluid Dynamics Conf., Cincinnati*, pp. 394–402.

GLOWINSKI, R. & PIRONNEAU, O. 1975 On the numerical computation of the minimum drag profile in laminar flow. *J. Fluid Mech.* **72**, 385–389.

GOLDSTEIN, R. J. & KREID, D. K. 1967 Measurement of laminar flow development in a square duct using a laser-Doppler flowmeter. *Trans. ASME* E: *J. Appl. Mech.* **89**, 813–818.

HENNE, P. A. 1980 An inverse transonic wing design method. *AIAA Paper* 80-0330.

HICKS, R. M. & HENNE, P. A. 1979 Wing design by numerical optimization. *AIAA Paper* 79-0080.

HIRSCH, C. 1990 *Numerical Computation of Internal and External Flows*, vol. 2, p. 603. John Wiley.

JAMESON, A. 1988 Aerodynamic design via control theory. *NASA ICASE Rep.* 88-64.

JAMESON, A., SCHMIDT, W. & TURKEL, E. 1981 Numerical solutions of the Euler equations by finite volume methods using Runge–Kutta time-stepping schemes. *AIAA Paper* 81-1259.

KREISS, H.-O. & LORENZ, J. 1989 *Initial-Boundary Value Problems and the Navier–Stokes Equations*, pp. 347–349. Academic.

LIGHTHILL, M. J. 1945 A new method of two dimensional aerodynamic design. *Aero. Res. Counc. R and M* 2112.

LIONS, J. L. 1968 *Contrôle Optimal de Systèmes Governés par des Equations aux Derivées Partielles.* Paris: Dunod.

LIONS, J. L. & MAGENES, E. 1967 *Problémes aux Limites Non-homogènes*, vol. 1. Paris: Dunod.

MCFADDEN, G. B. 1979 An artificial viscosity method for the design of supercritical airfoils. *New York University Rep.* C00-3077-158.

PIRONNEAU, O. 1973 On optimum profiles in Stokes flow. *J. Fluid Mech.* **59**, 117–128.

PIRONNEAU, O. 1974 On optimum design in fluid mechanics. *J. Fluid Mech.* **64**, 97–110.

RIZZI, A. & ERIKSSON, L.-E. 1984 Computation of flow around wings based on the Euler equations. *J. Fluid Mech.* **148**, 45–71.

RIZZI, A. & ERIKSSON, L.-E. 1985 Computation of inviscid incompressible flow with rotation. *J. Fluid Mech.* **153**, 275–312.

SUNG, C.-H. 1987 An explicit Runge–Kutta method for 3D turbulent incompressible flows. *David W. Taylor Naval Ship Research and Development Center, Ship Hydromechanics Department Rep.* DTNSRDC/SHD-1244-01.

SWANSON, R. C. & TURKEL, E. 1985 A multistage time-stepping scheme for the Navier–Stokes equations. *AIAA Paper* 85-35.

THOMPSON, J. F., THAMES, F. C. & MASTIN, C W. 1974 Automatic numerical generation of body-fitted curvilinear coordinate system for field containing any number of arbitrary two-dimensional bodies. *J. Comput. Phys.* **15**, 299–319.

TRANEN, J. L. 1974 A rapid computer aided transonic airfoil design method. *AIAA Paper* 74-501.

TUCK, E. O. 1968 *Proc. Conf. Hydraul. Fluid Mech.*, p. 29. Australia: Institute of Engineers.

VATSA, V. N. 1986 Accurate solutions for transonic viscous flow over finite wings. *AIAA Paper* 86-1052.

VOLPE, G. & MELNIK, R. E. 1986 The design of transonic aerofoils by a well posed inverse method. *Intl J. Numer. Methods Engng* **22**, 341–361.

WATSON, S. R. 1971 Towards the minimum drag on a body of given volume in slow viscous flow. *J. Inst. Maths Applics.* **7**, 367–376.